

Journal of Applied Remote Sensing

RemoteSensing.SPIEDigitalLibrary.org

Synthetic aperture radar image change detection based on frequency- domain analysis and random multigraphs

Feng Gao
Xiao Wang
Junyu Dong
Shengke Wang

SPIE.

Feng Gao, Xiao Wang, Junyu Dong, Shengke Wang, "Synthetic aperture radar image change detection based on frequency-domain analysis and random multigraphs," *J. Appl. Remote Sens.* **12**(1), 016010 (2018), doi: 10.1117/1.JRS.12.016010.

Synthetic aperture radar image change detection based on frequency-domain analysis and random multigraphs

Feng Gao, Xiao Wang, Junyu Dong,* and Shengke Wang

Ocean University of China, Department of Computer Science and Technology, Qingdao, China

Abstract. With the development of earth observation programs, many multitemporal synthetic aperture radar (SAR) images over the same geographical area are available. It is demanding to develop automatic change detection techniques to take advantage of these images. Most existing techniques directly analyze the difference image (DI), and therefore, they are easily affected by the speckle noise. We proposed an SAR image change detection method based on frequency-domain analysis and random multigraphs. The proposed method follows a coarse-to-fine procedure: in the coarse changed regions localization stage, frequency-domain analysis is utilized to select distinctive and salient regions from the DI. Therefore, nonsalient regions are neglected, and noisy unchanged regions incurred by the speckle noise are suppressed. In the fine changed regions classification stage, random multigraphs are employed as the classification model. By selecting a subset of neighborhood features to create graphs, the proposed method can efficiently exploit the nonlinear relations between multitemporal SAR images. The experimental results on two real SAR datasets and one simulated dataset have demonstrated the effectiveness of the proposed method. © 2018 Society of Photo-Optical Instrumentation Engineers (SPIE) [DOI: 10.1117/1.JRS.12.016010]

Keywords: random multigraphs; saliency map; synthetic aperture radar; change detection; frequency-domain analysis.

Paper 170440 received May 23, 2017; accepted for publication Dec. 12, 2017; published online Jan. 11, 2018.

1 Introduction

With the advance of earth observation programs, many synthetic aperture radar (SAR) sensors have been developed for modern spaceborne systems. More and more multitemporal SAR images over the same geographical area are available. Therefore, change detection using SAR images has drawn increasing attention in remote sensing communities. SAR image change detection is of high practical value to a large number of applications, such as disaster monitoring,¹ flood detection,² concealed target detection,³ urban planning,⁴ land cover data updating,⁵ and so on.

SAR sensors create images by illuminating a scene with successive pulses of radio waves and processing the received echoes.⁶ They are independent of atmospheric and sunlight conditions.⁷ Therefore, SAR images are the ideal and indispensable source to detection land cover changes. Especially, when heavy rain causes severe flooding, SAR images can make up for the shortage of effective optical, infrared, and LiDAR remote sensing images.⁸ However, the SAR images are inherently contaminated by multiplicative speckle noises,⁹ and this phenomenon makes the SAR image change detection a very challenging task. Therefore, it is important to develop robust change detection techniques, which can cope with the speckle noise.¹⁰

To cope with the speckle noise, many methods have been proposed for SAR image change detection. These methods can be categorized into two main streams: the supervised method^{11,12} and the unsupervised method.^{13–15} The supervised method requires knowledge about the land cover types or labeled samples collected by experts. Liu et al.¹¹ proposed a supervised method to detection changes of bare lands, lawns, and water using some labeled samples. In theory,

*Address all correspondence to: Junyu Dong, E-mail: dongjunyu@ouc.edu.cn

supervised method may have better performance in obtaining better description of the changes. However, a lack of qualified labeled samples in real applications makes the unsupervised method more popular than the supervised method.¹⁶ In this paper, we mainly focus on the unsupervised SAR image change detection methods.

Generally, the unsupervised SAR image change detection can be divided into three steps: (1) image preprocessing; (2) generation of the difference image (DI); and (3) analysis of the DI. The first step usually includes geometric correction and registration. In practice, the residual registration noises will affect the performance of change detection.¹⁵ In this paper, we assume that the input multitemporal images have been coregistered, and then we mainly focus on the process of DI generation and analysis. In the DI generation step, the log-ratio operator is one of the most widely used methods since it is considered to have the capability to transform multiplicative speckle noise into an additive one. Hence, the DI generated by log-ratio operator is robust to calibration and radiometric errors. In the DI analysis step, the pixels are classified into changed and unchanged classes using thresholding,¹⁷ fuzzy c-means (FCM) clustering,¹⁸ Markov fusion,¹⁹ etc. Celik²⁰ used principal component analysis (PCA) to construct an eigenvector space on the DI. Then, k-means clustering is adopted to cluster the features into changed and unchanged. Gong et al.²¹ took spatial information into account and proposed an improved FCM clustering for SAR image change detection. In recent years, Markov random fields²² and multistage extreme learning machine²³ were also applied to solve the change detection problem. Yousif and Ban²² utilized Markov random field to model the local interactions between pixels' labels. The model has the potential to preserve spatial details and to reduce speckle effects. Jia et al.²³ used a multistage extreme learning machine to model the spatial-neighborhood information between multitemporal SAR images. Most existing methods focus on building a robust classification model for DI analysis. However, there are many noisy regions in the DI that are generated by the speckle noise. Therefore, the performance of existing methods is usually affected by these noisy regions. Removing these noisy regions before DI analysis may improve the performance of change detection.

Two important problems need to be considered in SAR image change detection. First, the noisy regions in the DI must be neglected or suppressed. Second, a good classification model is needed for changed region classification.

For the first problem, changed regions in the DI usually have higher gray values than unchanged regions, which make the changed regions much more distinctive and salient. This phenomenon inspires us to use saliency detection methods to suppress the noisy regions in the DI. In this paper, frequency-domain analysis²⁴ is employed to generate a salient map of the DI. In the salient map, many noise unchanged regions are suppressed. With respect to the second problem, graph-based methods have recently received significant attention due to their efficiency.^{25,26} These methods utilize a graph structure to constrain the classification function to be smooth. In our previous work, we proposed a random multigraphs method,²⁷ which is a graph-based method to solve the problem of data classification. Inspired by the random forest algorithm,²⁸ randomly selecting a subset of features to create a graph can avoid the problem of overfitting. Hence, the performance of classification can be improved. In this paper, we introduce the idea of random multigraphs into SAR images to exploit the nonlinear relationship between multitemporal SAR images, and the speckle noise can be suppressed to some extent.

In this paper, we proposed a change detection method for SAR image change detection based on frequency-domain analysis and random multigraphs. First, by observing that the phenomenon that truly changed regions in the DI is salient and distinctive, we utilized frequency-domain analysis²⁴ to obtain salient changed regions. Then, FCM is used to select reliable samples from these regions. Neighborhood features of the pixels in the salient changed regions are fed into the random multigraphs for classification. Through classification, pixels in the DI are classified into changed class and unchanged class, and, thus, the final change map can be obtained.

The main contributions of the proposed method are threefold: first, we use frequency-domain analysis to find the salient changed regions from the SAR images, which is different from the existing methods. Second, we introduce a random multigraphs algorithm for SAR image change detection for the first time. Random multigraphs combine the ideas of random forest and anchor graph, which will contribute to classification performance improvements. Third, we proposed

a new coarse-to-fine framework for multitemporal SAR image change detection. The framework is composed of coarse changed regions localization and fine changed regions classification. Experimental results on three real SAR datasets demonstrate the effectiveness of the proposed method.

The remainder of this paper is organized as follows. Section 2 gives the problem statements and some background knowledge. Section 3 presents the detailed description of the proposed change detection method. Section 4 presents the experimental results of the proposed method and closely related methods on three real SAR datasets. Finally, Sec. 5 gives the concluding remarks of the proposed method.

2 Background

In this section, the problem of SAR image change detection is briefly described, and the motivation of the proposed method is presented. Then, frequency-domain analysis and random multigraphs are described in detail.

2.1 Problem Statements and Motivation

Consider two coregistered multitemporal SAR images I_1 and I_2 , and both images are contaminated with multiplicative speckle noise. The purpose of change detection is to generate a change map, which represents the changes that occur between I_1 and I_2 . From another point of view, the problem of SAR image change detection can be viewed as a binary classification process. After classification, we obtain a binary image in which unchanged pixels are labeled with 0 and changed pixels are labeled with 1.

As mentioned before, in this paper, the process of change detection includes two stages: coarse changed regions localization and fine changed regions classification. In the first stage, we use frequency-domain saliency detection²⁴ to suppress noisy unchanged regions in the DI. In the second stage, a random multigraphs algorithm provides a good solution of changed and unchanged pixels classification. Next, the frequency-domain analysis is introduced in Sec. 2.2, and the random multigraphs algorithm is described in Sec. 2.3.

2.2 Introduction to Frequency-Domain Saliency Detection

Saliency detection means finding the regions that exhibit a strong local or global contrast. As shown in Fig. 1(a), the changed regions are bright regions that are quite distinctive. These regions attract greater attention by the human visual system than other parts of the image. Figure 1(b) shows the saliency map generated by frequency-domain analysis, and Fig. 1(c) shows the ground-truth change map. It can be observed that the shape and position of the salient regions are similar to the changed regions. Therefore, frequency-domain saliency detection is suited for coarse changed regions localization.

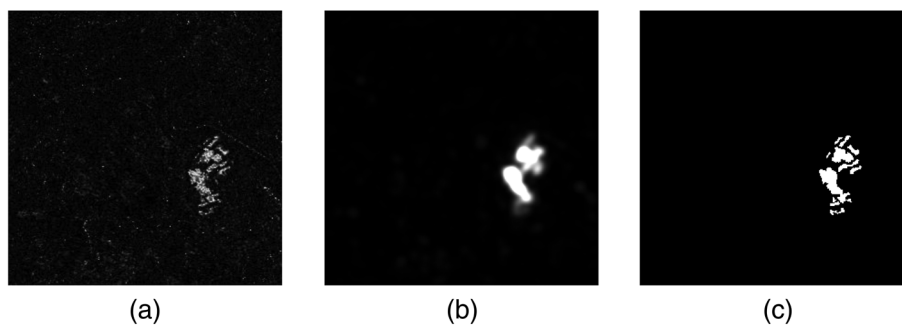


Fig. 1 The similarity between the saliency map and the ground-truth change map. (a) DI obtained by the log-ratio operator. (b) Saliency map generated by the frequency-domain analysis. (c) Ground-truth change map produced via manual marking by the combination of prior knowledge and photo interpretation.

Frequency-domain saliency detection uses a low-pass Gaussian kernel with an appropriate scale for amplitude spectrum convolution and then obtains the saliency map. Specifically, given an image $f(x, y)$, it was first transformed into the frequency domain by Fourier transform: $f(x, y) \rightarrow \mathcal{F}(f)(u, v)$. The amplitude spectrum $\mathcal{A}(u, v) = |\mathcal{F}(f)|$ and the phase spectrum $\mathcal{P}(u, v) = \text{angle}[\mathcal{F}(f)]$ are computed. A Gaussian kernel h is employed to suppress spikes in the amplitude spectrum $|\mathcal{F}(f)|$ of an image as follows:

$$\mathcal{A}_S(u, v) = |\mathcal{F}(f)| * h. \tag{1}$$

The resulting smoothed amplitude spectrum \mathcal{A}_S and the original phase spectrum are combined to compute the inverse transform, which in turn, yields the saliency map:

$$\mathcal{S} = \mathcal{F}^{-1}\{\mathcal{A}_S(u, v)e^{i\mathcal{P}(u,v)}\}. \tag{2}$$

2.3 Introduction to Random Multigraphs

There are many methods proposed to solve the classification problems in remote sensing image applications.²⁹⁻³¹ However, graph-based classification methods are rarely used in SAR image processing. In this paper, in the fine changed regions classification stage, we use random multigraphs²⁷ to classify the pixels in the changed region candidates into changed and unchanged classes. It can exploit the nonlinear relationship between multitemporal SAR images by randomly select a subset of features to create graphs.

The random multigraphs method uses an undirected graph to model the input data and the relationship among the data. Given a dataset $X = X_l \cup X_u \in \mathbb{R}^d$, d is the dimension of the feature space. $X_l = \{x_1, x_2, \dots, x_l\}$ is a labeled set with the labels $y_i \in \{0,1\}$. $X_u \in \{x_{l+1}, \dots, x_{l+u}\}$ is an unlabeled set, and u is the number of unlabeled data.

Figure 2 illustrates the flowchart of the random multigraph algorithm. The whole framework of random multigraph can be described as follows:

- Step 1: Randomly select k_f features from all the d -dimensional features of each sample.
- Step 2: Select m anchor points to cover the data manifold denoted by anchors matrix \mathbf{A} and then compute the mapping matrix \mathbf{P} to represent the rest of the data points via the selected anchors.
- Step 3: Run inference on this graph using graph Laplacian regularization.
- Step 4: Go to step 1, until we obtain k_g graphs.
- Step 5: The obtained k_g graphs are chosen to get the labels for the unlabeled data points.

In this paper, we use the anchor graph method³² to construct graphs. $\mathbf{A} = \{a_j\}_{j=1}^m \in \mathbb{R}^d$ in which each a_j is an anchor point. As such, the label prediction function f can be represented as follows:

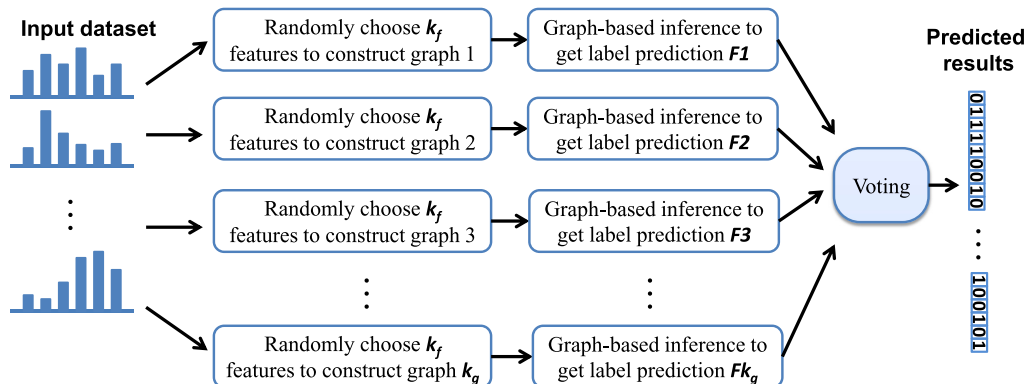


Fig. 2 Flowchart of the random multigraphs method.

$$f(x_i) = \sum_{j=1}^m \mathbf{P}_{ij} f(a_j), \tag{3}$$

where \mathbf{P}_{ij} is the data-adaptive weight. Define two vectors $\mathbf{f} = [f(x_1), \dots, f(x_n)]^T$ and $\mathbf{f}_a = [f(a_1), \dots, f(a_m)]^T$; the above equation can be rewritten as follows:

$$\mathbf{f} = \mathbf{P}\mathbf{f}_a, \mathbf{P} \in \mathbb{R}^{(l+u) \times m}, \quad m \ll l + u. \tag{4}$$

Thus, the solution space of unknown labels is reduced from the larger space f to a smaller space f_a . We use k-means clustering centers as anchors. It is believed that these clustering centers have strong representation power to adequately cover the full dataset.

With respect to the matrix \mathbf{P} , we use local anchor embedding³² to reconstruct any data point as a convex combination of its closest anchors. Therefore, the matrix \mathbf{P} can be determined by

$$\min J(\mathbf{P}) = \frac{1}{2} \|\mathbf{X} - \mathbf{P}\mathbf{A}\|^2 \quad \text{s.t. } \mathbf{P}_{ij} \geq 0, \mathbf{P}_i \mathbf{1} = 1, \tag{5}$$

where \mathbf{X} denotes a data matrix in which every row is a data sample. $\mathbf{A} \in \mathbb{R}^{(l+u) \times d}$ is the anchor matrix in which every row is an anchor. $\mathbf{P} \in \mathbb{R}^{(l+u) \times m}$ is the data-anchor mapping matrix, which is to be learned. Using the matrix \mathbf{P} , the graph can be represented by its adjacency matrix $\mathbf{W} = \mathbf{P}\mathbf{A}^{-1}\mathbf{P}^T$. The diagonal matrix $\mathbf{\Lambda} \in \mathbb{R}^{m \times m}$ is defined as $\Lambda_{kk} = \sum_{i=1}^{l+u} \mathbf{P}_{ik}$.

After obtaining the mapping matrix \mathbf{P} , through a semisupervised learning framework, the labels of unlabeled data can be predicted easily. More detailed information can be found in Ref. 27.

3 Methodology

In this section, the detailed implementation of the proposed method is described. The overall framework of the proposed method is shown in Fig. 3. Specifically, the proposed change detection method is composed of two main stages:

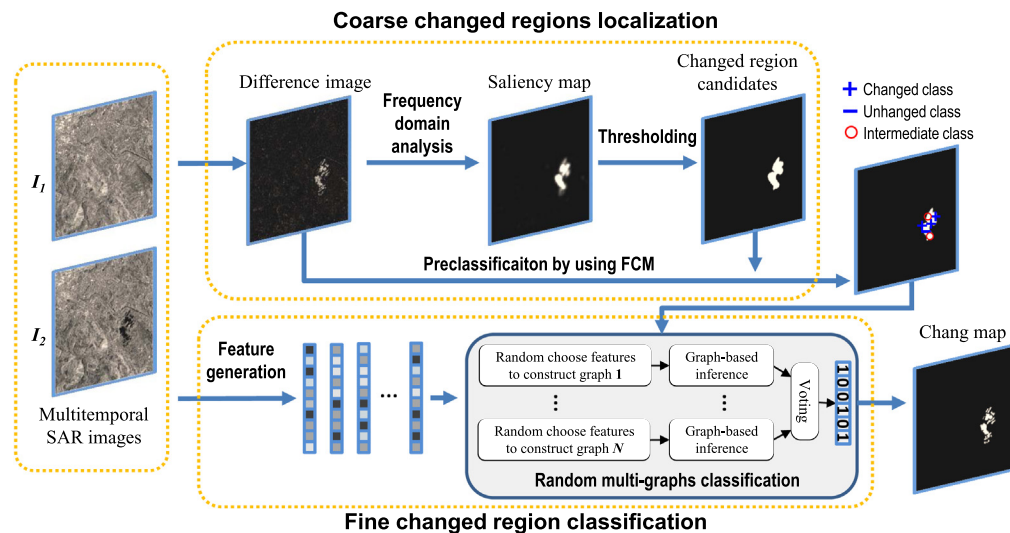


Fig. 3 Flowchart of the proposed SAR image change detection method based on frequency-domain analysis and random multigraphs. (a) The log-ratio operator is first used to generate a DI, and then frequency-domain analysis is utilized to obtain changed region candidates. (b) Representative sample pixels are selected from changed region candidates using FCM. Image patches are generated around each pixel, and these features are fed into random multi-graphs for classification. Finally, the final change map can be obtained from the classification results.

- Stage 1—Coarse changed regions localization using frequency-domain analysis. The log-ratio operator is first used to generate a DI. Then, frequency-domain analysis is utilized to obtain salient and distinctive regions. These regions are selected as changed region candidates and will be further classified in Stage 2.
- Stage 2—Fine changed regions classification based on random multigraphs. Representative samples pixels are selected from changed region candidates by FCM clustering. These pixels are treated as labeled samples. Image patch features are generated around each pixel, and these features are fed into random multigraphs for classification. From the classification result, we can get changed pixels and thus obtain the final change map.

3.1 Coarse Changed Regions Localization Based on Frequency-Domain Analysis

Given two multitemporal SAR images, $I_1 = \{I_1(i, j), 1 \leq i \leq M, 1 \leq j \leq N\}$ and $I_2 = \{I_2(i, j), 1 \leq i \leq M, 1 \leq j \leq N\}$. The log-ratio operator is utilized to generate the DI I_D . It is computed pixel-by-pixel from I_1 and I_2 by

$$I_D = |\log(I_1) - \log(I_2)|. \quad (6)$$

The changed regions in I_D are believed to be salient and distinctive by visual perception. Thus, we use the saliency detection method to locate changed region candidates. Frequency-domain analysis²⁴ is adopted here. It uses a low-pass Gaussian kernel for amplitude spectrum convolution and then obtains the change map. In our implementations, the input DI is resized to 256×256 pixels for Fourier transform. In addition, it is empirically verified that when the Gaussian kernel size is set to $0.05 \cdot N$ (here, N is the width of the input image), the saliency detector obtains the best performance. Thus, we set the kernel size as $0.05 \cdot N$ in our implementations.

After obtaining the saliency map, the thresholding method is utilized to generate changed region candidates. Specifically, pixels with a value greater than a given threshold t will be preserved as changed region candidates. After the thresholding operation, interest regions with salient and distinctive information will be extracted. These regions will be further classified by random multigraphs. It is well worth noting that t is an important parameter that can affect the change detection results. The analysis of the parameter will be described in detail in Sec. 4.

3.2 Fine Changed Regions Classification Based on Random Multigraphs

For fine changed regions classification, we first perform FCM algorithm on the changed region candidates in the DI to partition pixels into three clusters: changed class Ω_c , unchanged class Ω_u , and intermediate class Ω_i . Pixels belonging to Ω_c and Ω_u have high probability to be changed and unchanged. Specifically, Ω_c and Ω_u have higher within-class similarity and lower interclass similarity, and they can be viewed as pure changed and unchanged classes. Therefore, Ω_c and Ω_u can be treated as reliable labeled samples for random multigraphs.

The neighborhood features of all the pixels in changed region candidates (belonging to Ω_u , Ω_c , and Ω_i) are generated, as shown in Fig. 4. It is well worth noting that, since the properties of a pixel are highly correlated with its neighborhood, the corresponding patches in the multitemporal SAR images are extracted and stacked together as the feature vector of the pixel. Specifically, an image patch centered at (i, j) in image I_1 is extracted. The corresponding image patch in image I_2 is also extracted. Both image patches are converted to vectors V_{ij}^1 and V_{ij}^2 , respectively. Both vectors are concatenated and form a new vector V_{ij} . This process is illustrated in Fig. 4, and V_{ij} denotes the feature vector at the position (i, j) .

Therefore, we obtain neighborhood features of pixels in changed region candidates. These features are fed into the random multigraphs for classification. Pixels belonging to Ω_c and Ω_u are treated as labeled samples in classification. Through the semisupervised inference in random multigraphs, it can classify the unlabeled samples into changed class or unchanged class. From the classification result, we can obtain the final change detection result.

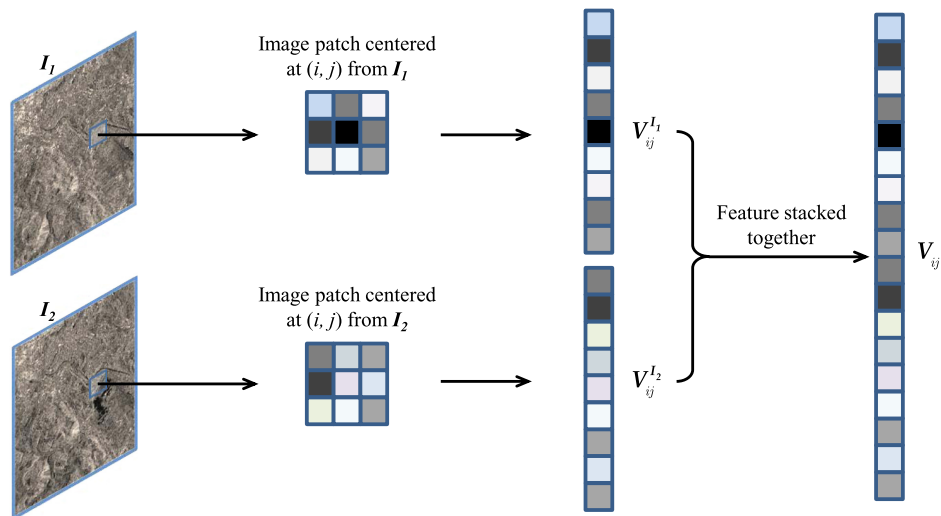


Fig. 4 Neighborhood feature generation of each position as the input of random multigraphs.

4 Experimental Result and Analysis

In this section, we evaluate the proposed method on two real SAR datasets and one simulated dataset. We also compare the proposed method with some existing change detection techniques to demonstrate its superiority.

4.1 Dataset Description and Experimental Settings

The first dataset utilized in the experiment is the Bern dataset. As shown in Fig. 5, it consists of two SAR images captured by ERS-2 satellite. The images were captured in April and May 1999, respectively. During the period between these two dates, the River Aare flooded parts of Bern. The available ground truth, as shown in Fig. 5(c), was produced via manual marking by the combination of prior knowledge and photo interpretation.

The second dataset used in the experiment is the San Francisco dataset, as shown in Fig. 6. It represents a section (256×256 pixels) of two SAR images over the city of San Francisco acquired by ERS-2 SAR sensor. The dataset contains two images acquired in August 2003 and May 2004, respectively. The original images are 7749×7713 pixels and are available in Earthnet.³³ The available ground truth, as shown in Fig. 6(c), was produced by integrating prior knowledge and photo interpretation.

The third dataset, as shown in Fig. 7, is a simulated dataset. The size of the dataset is 256×256 pixels. The ground truth is shown in Fig. 7(c). The simulated dataset is partly from a panchromatic IKONOS image of Beijing, China. Nakagami-distributed speckle patterns have been synthesized with chosen parameters, and these patterns have been added into the

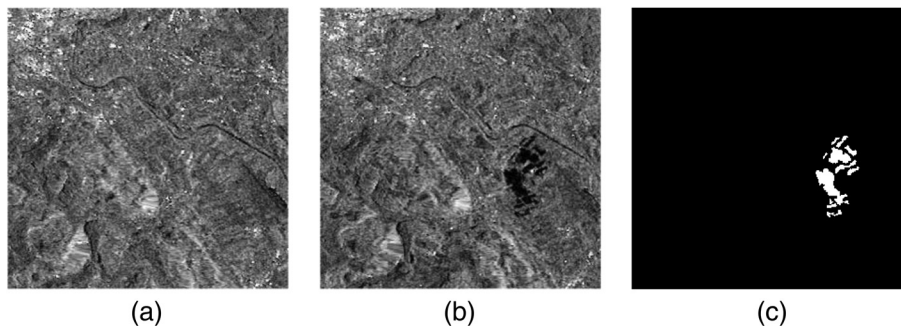


Fig. 5 Bern dataset: (a) image acquired in April 1999, (b) image acquired in May 1999, and (c) ground-truth image produced via manual marking by the combination of prior knowledge and photo interpretation.

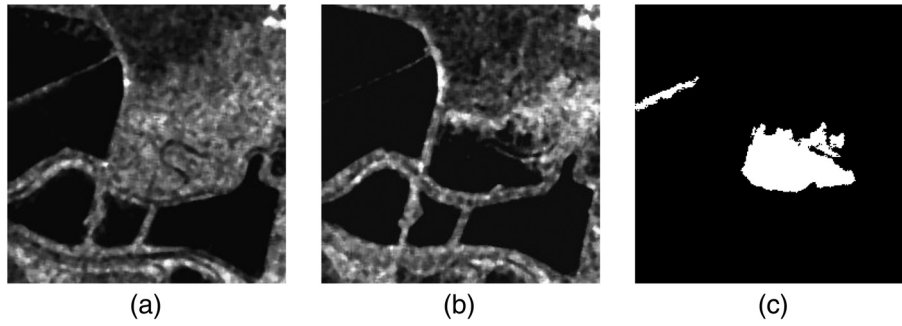


Fig. 6 San Francisco dataset: (a) image acquired in August 2003, (b) image acquired in May 2004, and (c) ground-truth image produced by integrating prior knowledge and photo interpretation.

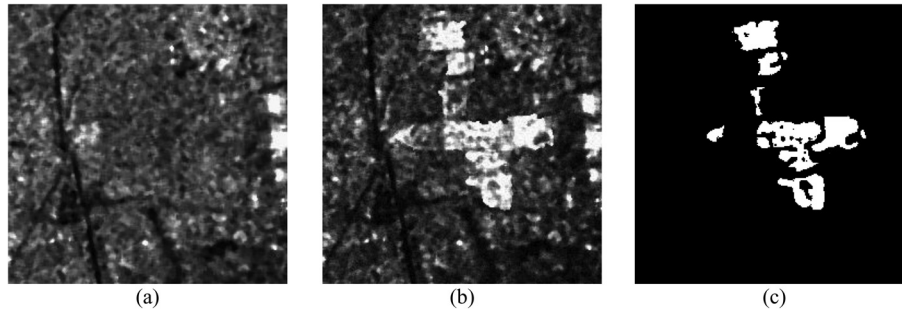


Fig. 7 Simulated dataset: (a) image changed before, (b) image changed after, and (c) ground-truth image generated via manual marking by integrating prior information with photo interpretation.

image as speckle noise. The changed regions in Fig. 7(b) have ~40% enhancement in the amplitude levels compared with the corresponding regions in Fig. 7(a).

The change detection results are shown in the form of binary maps, while the white pixels denote the changed pixels and the black pixels denote the unchanged pixels. The quantitative analysis is made on the change detection results to evaluate the performance of the proposed method. False positive (FP) and false negative (FN) are first calculated. FP is the number of pixels that are unchanged class in the ground-truth image but wrongly classified as changed ones. FN is the number of pixels that are changed class in the ground-truth image but wrongly classified as unchanged ones. Next, we compute the overall error (OE) and the percentage correct classification (PCC). The OE is computed by $OE = FN + FP$. The PCC is computed by $PCC = (TP + TN) / (TP + TN + FP + FN) \times 100\%$, where TN denotes the true negative, which is the number of pixels correctly classified as unchanged ones, and TP denotes the true positive, which is the number of pixels correctly classified as changed ones. Finally, the kappa coefficient³⁴ is computed to give the percentage of agreement (correct classified pixels) corrected by the number of agreements that would be expected purely by chance. Specifically, kappa coefficient (KC) is calculated by PCC and Proportional Reduction in Error (PRE) as follows:

$$KC = \frac{PCC - PRE}{1 - PRE}, \quad (7)$$

where

$$PRE = \frac{(TP + FP) \cdot (TP + FN)}{(TP + TN + FP + FN)^2} + \frac{(FN + TN) \cdot (FP + TN)}{(TP + TN + FP + FN)^2}. \quad (8)$$

The proposed method is compared with closely related methods on three SAR datasets. The methods used for comparison purpose are principal component analysis and k-means clustering (PCA KM),²⁰ Markov random field and fuzzy c-means clustering (MRFFCM),³⁵

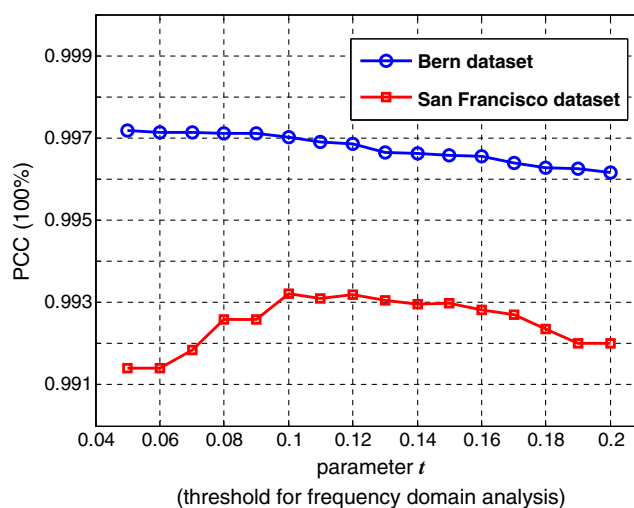


Fig. 8 Relationship between PCC and the parameter t on two real SAR datasets.

Gabor feature extractoin and two-level clustering (GaborTLC),¹⁸ and nearest neighbor - extreme learning machines (NR-ELM).¹⁵ The results of these methods are implemented using the authors' publicly available codes. The MATLAB implementation of the proposed method is available at Ref. 36. The experimental results of these methods on three SAR datasets will be discussed in the following subsections.

4.2 Test of the Parameter t

The first experiment is a test of the parameter t . t stands for the threshold for frequency-domain analysis. It is an important parameter that can affect the final change detection results. Figure 8 shows the relationship between PCC and the parameter t on two real SAR datasets. Take the results on the Bern dataset as an example; the PCC values are almost the same when t ranges from 0.04 to 0.10. When t is larger than 0.11, the PCC value decreases slightly. On the San Francisco dataset, the value of PCC increases when t ranges from 0.04 to 0.11. This is because, when t is relatively small, many noisy regions will be retained. These noisy regions affect the performance of change detection. However, when t is larger than 0.12, the value of PCC decreases. When the value of t becomes larger, the size of extracted salient regions will be very small and many real changed regions will be neglected. From the results on both datasets, we observe that when t ranges from 0.10 to 0.12, the value of PCC is stable and satisfying. Therefore, in our implementations, we set the value of t as 0.11.

4.3 Experimental Results on the Bern Dataset

The experimental results are exhibited in two ways: the final change maps in figure form and the quantitative analysis in tabular form. Figure 9 shows the final change maps of various methods on the Bern dataset, and Table 1 lists the values for evaluation.

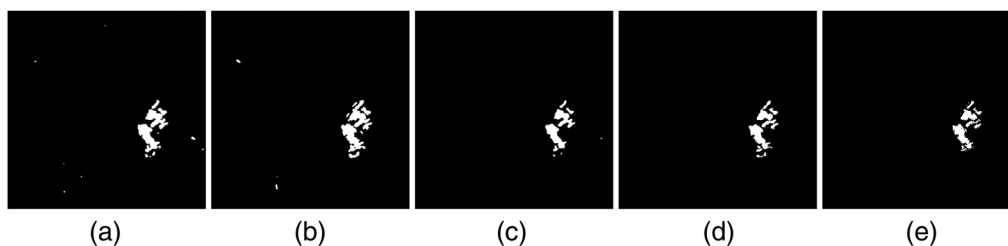


Fig. 9 Visualized results of various change detection methods on the Bern dataset: (a) result by PCAKM,²⁰ (b) result by MRFFCM,³⁵ (c) result by GaborTLC,¹⁸ (d) result by NR-ELM,¹⁵ and (e) result by the proposed method.

Table 1 Change detection results of different methods on the Bern dataset.

Methods	FP	FN	OE	PCC (%)	KC (%)
PCAKM ²⁰	247	119	366	99.60	84.78
MRFFCM ³⁵	364	47	411	99.55	84.13
GaborTLC ¹⁸	135	173	308	99.66	86.27
NR-ELM ¹⁵	147	146	293	99.68	87.16
Proposed method	55	216	271	99.70	87.24

As shown in Figs. 9(a) and 9(b), the PCAKM and MRFFCM wrongly classify some unchanged pixels into the changed class, which generates some noisy regions. Therefore, the FP values of PCAKM and MRFFCM are relatively high, as shown in Table 1. As mentioned before, the proposed method utilized frequency-domain analysis to generate a salient map of the DI; then, many noisy unchanged regions are suppressed. Therefore, the proposed method works well in suppressing background noise and achieves the minimum FP value. In addition, the proposed method achieves the maximum PCC and KC values. It is well worth noting that the PCC and KC values are persuasive coefficients in change detection results analysis. Thus, we can draw the conclusion that the proposed method outperforms the other methods on the Bern dataset.

4.4 Experimental Results on the San Francisco Dataset

The change detection results of different methods on the San Francisco dataset are shown in Fig. 10. The corresponding quantitative metrics on the change maps generated by different methods are shown in Table 2. From the visual comparison among these change maps, we can observe that the PCAKM, MRFFCM, and GaborTLC generate many noise regions, and, in these regions, many unchanged pixels are falsely classified into the changed class. Thus, the FP values of these methods are relatively high. High FP values affect the overall performance of these methods. The NR-ELM and the proposed method obtain similar lower FP values compared with the above-mentioned methods, as shown in Table 2. However, the FN values of the proposed method are much lower than NR-ELM. Thus, the proposed method achieves the best PCC and KC values. Results on this dataset also demonstrate that noisy unchanged regions can be suppressed by the proposed method. Both visual and quantitative analyses demonstrate the effectiveness of the proposed method on the dataset.

4.5 Experimental Results on the Simulated Dataset

As for the simulated dataset, the results are shown in Fig. 11 and listed in Table 3. The effects of speckle noise are quite strong on the dataset. From Fig. 11, we can observe that many unchanged pixels are falsely classified into the changed class by PCAKM, MRFFCM, GaborTLC, and

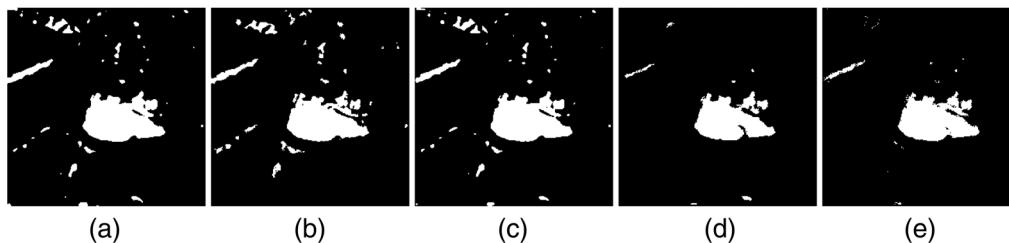
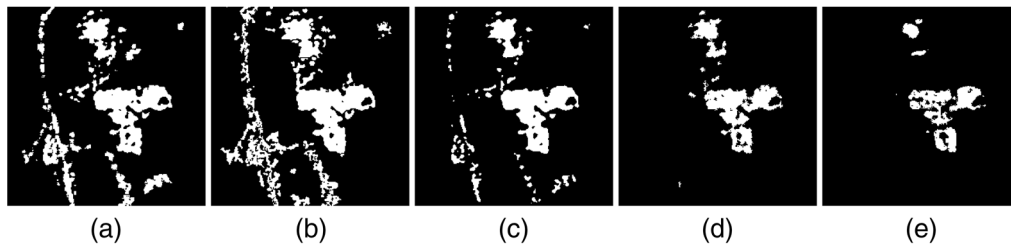


Fig. 10 Visualized results of various change detection methods on the San Francisco dataset: (a) result by PCAKM,²⁰ (b) result by MRFFCM,³⁵ (c) result by GaborTLC,¹⁸ (d) result by NR-ELM,¹⁵ and (e) result by the proposed method.

Table 2 Change detection results of different methods on the San Francisco dataset.

Methods	FP	FN	OE	PCC (%)	KC (%)
PCAKM ²⁰	1618	25	1643	97.49	83.68
MRFFCM ³⁵	1511	191	1702	97.40	82.69
GaborTLC ¹⁸	1376	60	1436	97.81	85.39
NR-ELM ¹⁵	182	596	778	98.81	90.68
Proposed method	189	255	444	99.32	94.86

**Fig. 11** Visualized results of various change detection methods on the simulated dataset: (a) result by PCAKM,²⁰ (b) result by MRFFCM,³⁵ (c) result by GaborTLC,¹⁸ (d) result by NR-ELM,¹⁵ and (e) result by the proposed method.**Table 3** Change detection results of different methods on the simulated dataset.

Methods	FP	FN	OE	PCC (%)	KC (%)
PCAKM ²⁰	5588	544	6132	90.94	50.81
MRFFCM ³⁵	6883	232	7115	89.14	48.67
GaborTLC ¹⁸	2866	570	3436	94.76	65.91
NR-ELM ¹⁵	1090	897	1987	96.97	87.40
Proposed method	154	1364	1518	97.68	89.26

NR-ELM. Hence, the FP values of these methods are relatively high in Table 3. However, the proposed method can effectively suppress the speckle noise and achieves the lowest FP value. In addition, the KC value is obviously higher than the other methods, which means the proposed method is effective in strong speckle noise scenarios.

4.6 Discussion

The proposed method is a promising tool for detecting changed regions from multitemporal SAR images. As shown in Tables 1–3, the proposed method has better performance than four closely related methods. The methods used for comparison are PCAKM, MRFFCM, GaborTLC, and NR-ELM.

From the quantitative analysis listed in Tables 1–3, the proposed method achieves the smallest OE values and the maximum KC values. False positives generated by speckle noise appear to be nonsalient regions in the DI, and they are neglected in the process of frequency-domain analysis. Therefore, the proposed method achieves the best performance in FP values on three datasets. Moreover, random multigraphs randomly select a subset of neighborhood features to create graphs; it can exploit the nonlinear relations between multitemporal SAR images and therefore

suppress the speckle noise to some extent. It is evident that the proposed method is good at suppressing the noisy unchanged regions while preserving details.

5 Conclusion

In this paper, we proposed an SAR image change detection method based on frequency-domain analysis and random multigraphs. The proposed method follows a coarse-to-fine procedure: in the coarse changed regions localization stage, the log-ratio operator is first used to generate a DI. Then, frequency-domain analysis is utilized to obtain changed region candidates. In the fine changed regions classification stage, representative samples are selected from changed region candidates using FCM. Then, image patch features are generated around each pixel, and these features are fed into random multigraphs for classification. From the classification result, we can obtain the final changed map. The experimental results on both visual and quantitative analysis have demonstrated the effectiveness of the proposed method.

Acknowledgments

The authors would like to thank the editors and all the anonymous reviewers for their very competent comments and helpful suggestions. This work was supported by the National Natural Science Foundation of China (Grant Nos. 41606198, 61271405, 61576011, and 61401413) and in part by the Shandong Province Natural Science Foundation of China under Grant No. ZR2016FB02.

References

1. S. Martinis, A. Twele, and S. Voigt, "Unsupervised extraction of flood induced backscatter changes in SAR data using Markov image modeling on irregular graphs," *IEEE Trans. Geosci. Remote Sens.* **49**(1), 251–263 (2011).
2. D. Huong and R. Nagasawa, "Potential flood hazard assessment by integration of ALOS PALSAR and ASTER GDEM: a case study for the Hoa Chau commune, Hoa Vang district, in central Vietnam," *J. Appl. Remote Sens.* **8**(1), 083626 (2014).
3. G. Gao et al., "Modified log-ratio operator for change detection of synthetic aperture radar targets in forest concealment," *J. Appl. Remote Sens.* **8**(1), 083583 (2014).
4. C. Pratola et al., "Toward fully automatic detection of changes in suburban areas from VHR SAR images by combining multiple neural-network models," *IEEE Trans. Geosci. Remote Sens.* **51**(4), 2055–2066 (2013).
5. D. C. Zanotta and V. Haertel, "Gradual land cover change detection based on multitemporal fraction images," *Pattern Recognit.* **45**(2), 2927–2937 (2012).
6. H. Aghababae, Y.-C. Tzeng, and J. Amini, "Swarm intelligence and fractals in dual-pol synthetic aperture radar image change detection," *J. Appl. Remote Sens.* **6**(1), 063596 (2012).
7. H. Hu and Y. Ban, "Unsupervised change detection in multitemporal SAR images over large urban areas," *IEEE J. Sel. Top. Appl. Earth Obs. Remote Sens.* **7**(8), 3248–3261 (2014).
8. B. Hou et al., "Unsupervised change detection in SAR image based on gauss-log ratio image fusion and compressed projection," *IEEE J. Sel. Top. Appl. Earth Obs. Remote Sens.* **7**(8), 3297–3317 (2014).
9. F. Gao et al., "Automatic change detection in synthetic aperture radar images based on PCANet," *IEEE Geosci. Remote Sens. Lett.* **13**(12), 1792–1796 (2016).
10. J. Lu et al., "Difference representation learning using stacked restricted Boltzmann machines for change detection in SAR images," *Soft Comput.* **20**(12), 4645–4657 (2016).
11. M. Liu et al., "Polarimetric synthetic aperture radar change detection for specific land cover types," *Int. J. Digital Earth* **8**(4), 334–344 (2015).
12. G. Camps-Valls et al., "Kernel-based framework for multi-temporal and multi-source remote sensing data classification and change detection," *IEEE Trans. Geosci. Remote Sens.* **46**(6), 1822–1835 (2008).

13. L. Bruzzone and D. F. Prieto, "Automatic analysis of the difference image for unsupervised change detection," *IEEE Trans. Geosci. Remote Sens.* **38**(3), 1171–1182 (2000).
14. D. Gleich, "Markov random field models for non-quadratic regularization of complex SAR images," *IEEE J. Sel. Top. Appl. Earth Obs. Remote Sens.* **5**(3), 952–961 (2012).
15. F. Gao et al., "Change detection from synthetic aperture radar images based on neighborhood-based ratio and extreme learning machine," *J. Appl. Remote Sens.* **10**(4), 046019 (2016).
16. Y. Zheng et al., "Using combined difference image and k-means clustering for SAR image change detection," *IEEE Geosci. Remote Sens. Lett.* **11**(3), 691–695 (2014).
17. G. Moser and S. B. Serpico, "Generalized minimum-error thresholding for unsupervised change detection from SAR amplitude imagery," *IEEE Trans. Geosci. Remote Sens.* **44**(10), 2972–2982 (2006).
18. H. Li et al., "Gabor feature based unsupervised change detection of multitemporal SAR images based on low-level clustering," *IEEE Geosci. Remote Sens. Lett.* **12**(12), 2458–2462 (2015).
19. F. Melgani and Y. Bazi, "Markovian fusion approach to robust unsupervised change detection in remotely sensed imagery," *IEEE Geosci. Remote Sens. Lett.* **3**(4), 457–461 (2006).
20. T. Celik, "Unsupervised change detection in satellite images using principal component analysis and k-means clustering," *IEEE Geosci. Remote Sens. Lett.* **6**(4), 772–776 (2009).
21. M. Gong, Z. Zhou, and J. Ma, "Change detection in synthetic aperture radar images based on image fusion and fuzzy clustering," *IEEE Trans. Image Process.* **21**(4), 2141–2151 (2012).
22. O. Yousif and Y. Ban, "Improving SAR-based urban change detection by combining MAP-MRF classifier and nonlocal means similarity weights," *IEEE J. Sel. Top. Appl. Earth Obs. Remote Sens.* **7**(10), 4288–4300 (2014).
23. L. Jia et al., "SAR image change detection based on correlation kernel and multi-stage extreme learning machine," *IEEE Trans. Geosci. Remote Sens.* **54**(10), 5993–6006 (2016).
24. J. Li et al., "Visual saliency based on scale-space analysis in the frequency domain," *IEEE Trans. Pattern Anal. Mach. Intell.* **35**(4), 996–1010 (2013).
25. M. Belkin, P. Niyogi, and V. Sindhvani, "Manifold regularization: a geometric framework for learning from labeled and unlabeled examples," *J. Mach. Learn. Res.* **7**(1), 2399–2434 (2006).
26. K. Kim and S. Choi, "Label propagation through minimax paths for scalable semi-supervised learning," *Pattern Recognit. Lett.* **45**(1), 17–25 (2014).
27. Q. Zhang et al., "Random multi-graphs: a semi-supervised learning framework for classification of high dimensional data," *Image Vision Comput.* **60**, 30–37 (2017).
28. L. Breiman, "Random forests," *Mach. Learn.* **45**(1), 5–32 (2001).
29. Q. Wang, Z. Meng, and X. Li, "Local adaptive discriminative analysis for spectral-spatial classification of hyperspectral images," *IEEE Geosci. Remote Sens. Lett.* **14**(11), 2077–2081 (2017).
30. Y. Yuan, J. Lin, and Q. Wang, "Hyperspectral image classification via multi-task joint sparse representation and stepwise MRF optimization," *IEEE Trans. Cybern.* **46**(12), 2966–2977 (2016).
31. Q. Wang, J. Lin, and Y. Yuan, "Salient band selection for hyperspectral image classification via manifold ranking," *IEEE Trans. Neural Networks Learn. Syst.* **27**(6), 1279–1289 (2016).
32. W. Liu, J. He, and S. F. Chang, "Large graph construction for scalable semi-supervised graph-based method," in *Proc. Int. Conf. on Machine Learning*, pp. 679–686, (2010).
33. "Earthnet online," http://earth.esa.int/ers/ers_action/SanFrancisco_SAR_IM_Orbit_47426_20040516.html (11 May 2017).
34. R. L. Brennan and D. J. Prediger, "Coefficient kappa: some uses, misuses, and alternatives," *Educ. Psychol. Meas.* **41**, 687–699 (1981).
35. M. Gong et al., "Fuzzy clustering with a modified MRF energy function for change detection in synthetic aperture radar images," *IEEE Trans. Fuzzy Syst.* **22**(1), 98–109 (2014).
36. "Feng Gao's homepage," <http://fenggao.sinaapp.com> (30 December 2017).

Feng Gao is currently a lecturer at the College of Information Science and Engineering, Ocean University of China. He acquired his BS degree in software engineering from Chongqing University, China, in 2008, and received his PhD in computer science from Beihang University, China, in 2015. His research interests include information fusion, computer vision, and image understanding.

Xiao Wang received her BS degree in computer science from the Agriculture University of Qingdao, Qingdao, China, in 2013. Currently, she is pursuing her MS degree at Ocean University of China. Her research interests include SAR image change detection, anomaly detection on hyperspectral images, and applications.

Junyu Dong received his BS and MS degrees in applied mathematics from Ocean University of China in 1993 and 1999, respectively. He received his PhD in image processing in 2003 from the School of Mathematical and Computer Sciences, Heriot-Watt University, United Kingdom. He is currently a professor of computer science and the head of computer science and technology department at Ocean University of China.

Shengke Wang is an associate professor at the College of Information Science and Engineering, Ocean University of China. He acquired his BS degree in computer science from Jinan University, China, in 2000 and received his PhD in computer science from South China University of Technology, China, in 2005. His research interests include computer vision, machine learning, and image processing.